AEJ
Alexandria Engineering Journal

Simulation model for the orbital electrochemical hole sizing process

Essam Soliman
Production Eng. Dept., Faculty of Eng., Alexandria University, P.O. Box 21544, Alexandria, Egypt
E_soliman@alex.edu.eg

This work presents a simulation model for the orbital electrochemical sizing process. The model considers a rotating work part with a true hole. A disc like tool is fed through the hole and parallel to it axis. The tool and work part are modeled as stacks of thin discs. The work part is further divided into narrow radial segments. The tool and the hole are eccentric. Relations have been developed to determine the gap between each segment of the rotating work part and the moving tool at each point of time during process simulation. Relations for segment current and volumetric and linear machining rates are developed. The model is used to investigate the correlation between different process parameters and process performance measures. Process parameters include orbiting speed of the work part, feedrate, tool diameter, tool lip height and eccentricity. The performance measures include volumetric and linear removal rates and hole inaccuracy. Hole inaccuracy is represented by the average roundness and straightness errors of simulated hole surface. Simulation results showed that tool feedrate and work part orbiting speed have a negligible effect on volumetric and linear removal rates. However, they significantly affect hole inaccuracy. Increasing feedrate resulted in an increased hole inaccuracy, however, increasing orbiting speed resulted in a reduced hole inaccuracy. Also, it was found that a range of tool diameters should be avoided to ensure high volumetric removal rate. Increasing tool eccentricity resulted in increased volumetric and linear removal rates, and increased hole inaccuracy.

هذه الورقة البحثية تقدم نموذجا رياضيا لمحاكاة عملية ضبط الثقوب بالقطع الكهروكيميائي . النموذج يفترض عينة تدور بسرعة محددة وبها ثقب نافذ . ويفترض النموذج أداة قطع على شكل أسطوانة تمر داخل الثقب وفي اتجاه المحور بهدف ضبط الثقب ومع اعتبار وجود لا محورية بين الثقب وأداة القطع . تم وضع علاقات تربط الفراغ بين أداة القطع وسطح الثقب الداخلي وكذلك التيار المار من خلال المحلول الإلكتروليتي . الهدف من النموذج دراسة تأثير عوامل عملية القطع على معدل إزالة المعدن ودقة الثقب الناتج من خلال حساب عدم الدائرية المتوسطة للثقب . تشمل عوامل عملية القطع السرعة الدورانية للعينة ومعدل تغذية أداة القطع ونصف قطرها وسمكها . بالإضافة إلى قيم اللامحورية بين أداة القطع والثقب . وقد أظهرت محاكاة النموذج الرياضي أن معدل تغذية أداة القطع والسرعة الدورانية للعينة ليس لديهم تأثير يذكر على معدل إزالة المعدل لكن لهم تأثير واضح على عدم الدائرية المتوسطة . زيادة معدل تغذية أداة القطع يؤدي إلى زيادة عدم الدائرية المتوسطة في حين أن زيادة السرعة الدورانية للعينة يؤدى إلى إنقاصها . أظهرت المحاكاة أيضا أن مدى معين من نصف قطر أداة القطع يجب تجنبه لضمان رفع معدل إزالة المعدن وإنقاص عدم الدائرية المتوسطة . ومن نتائج المحاكاة أن زيادة لامحورية الثقب وأداة القطع وكذلك سمك أداة القطع يؤدي إلى زيادة معدل إزالة المعدن وإلى زيادة اللادائرية المتوسطة للثقب .

Keywords: Electrochemical machining, Orbital motion, Hole sizing, Modelling and simulation

1. Introduction

ElectroChemical Machining (ECM) is a metal removal process in which a DC volt is applied across a gap between a cathode electrode tool and an anode work part. A current passes through the electrolyte filled gap. The work part surface dissolves according to Faraday's law. The only reaction that takes place at the tool surface is gas evolution. The tool surface undergoes no erosion and retains its shape. High current densities involved in ECM result in heating of the electrolyte. High flow rate of electrolyte is necessary to keep its conductivity constant and to dispose machining debris.

ElectroChemical hole drilling and Sizing (ECS) processes are one class of ECM. They include jet, capillary, and electro-stream drilling. They have many applications, especially, in the aerospace, electronic and auto industries [1]. This is due to their ability to machine new hard materials without heat affected zones or residual stresses. Drilling of holes with large aspect ratio is another application of these processes. To further enhance these processes, orbiting tools are used Orbital ElectroChemical hole Sizing, (OECS) [2]. Orbiting tools can be stationary or feeding ones. Orbiting and feeding tools result in more efficient flow of electrolyte with minimum electrolyte heating effects. Also, disposal of machining debris is faster, thus, avoiding short circuit and gap variation problems.

Considerable research work has been conducted to simulate, control and experimentally enhance the ECS process performance. J. Kozak, et al. [3] developed a two dimensional model for the ECS process. They investigated the effects of machining parameters such as voltage, flow rate and properties of electrolyte on metal removal rate and current density. Experimental and theoretical results showed that metal removal rate is limited by the heating of electrolyte. Mohen et al. [4] reviewed the different ECS processes. They compared them with other hole drilling operations such as electrodischarge drilling and laser drilling. ECS processes have proven to be better from different comparison points such as aspect ratio and hole surface characteristics. S. Sharma et al. [5] investigated the electrochemical drilling of holes in Inconel super alloys using sodium chloride electrolyte. They created a hole in a multilayered work part by feeding an electrode tool towards it. They measured the hole diameter and hole roundness error at each layer as a measure of hole accuracy. They reported inconsistent variations in hole diameters, and reduced this inconsistency, together with roundness errors of the produced hole sections, to variations in process parameters.

H. Hocheng et al. [6] conducted experimental work to study the electrochemical polishing and brightening of holes using rotating and feeding electrodes. They used different rotating speeds at different feedrates. The authors concluded that an optimum set of machining parameters leads to better surface quality and shorter machining time compared with manual and machine lapping processes. Muasuzawa et al. [7] adopted the use of ECM mate electrode to remove the recast layer produced by wire electrodischarge machining. The use of such tool requires large power supply to provide the necessary current density over the entire electrode area. Low current densities could not produce the required surface quality.

Soliman et al. [8] developed a simulation methodology for the electrochemical profiling of through holes. They used an axially feeding tool with different feed functions. They pointed out that by controlling the feed rate complex hole profiles can be produced. J. Kozak, et al. [9] used a rotating tool electrode to ensure adequate electrolyte flow in gap and to eliminate the need for high electrolyte pressure. Using the rotating electrode, pressure changes within the gap were small, which resulted in a more stable machining process

M.S. Hewidy et al. [10] developed a model for the electrochemical drilling under orbital motion conditions. They conducted an experimental work to verify the model. Experimental and model simulation results were in good agreement. Results showed that using orbital motion enhances the accuracy of the machined hole. They also showed that current spikes due to debris accumulation in the gap diminished resulting in better surface finish. Z. Sadollah et al. [11] used an orbiting ECS electrode for finishing surfaces produced by electrodischarge machining. They noticed a reduction in the surface protrusion height at the flow ports. They also noticed an improvement in surface roughness with the increase of orbiting eccentricity and frequency. H. El-Hofy et al. [12-13] conducted experimental work to study the effect of different machining parameters on quality of holes produces by the OECM process using both stationary and feeding tools. The parameters included tool lip height, in case of feeding tools, and feedrate. They concluded that using orbiting tools results in good

surface finish, low roundness errors and efficient machining.

In the present paper, a model of the OECS process is developed and simulated for orbiting work part and feeding tool. The model is used for studying the effect of different machining parameters on volumetric and linear removal rate and inaccuracy of machined hole.

2. Process model

Fig. 1 shows a line sketch of the OECS process. A disc like tool of radius R_T and lip height H_T passes through a hole in a work part to adjust its dimension. The tool is modeled as a stack of N_T discs each of height h, $H_T = N_T \times h$, fig.1-a. The work part is modeled as a stack of N_W discs each of the height h. The height of the work part is $H_w = N_w \times h$. The work part is further divided into S_W radial segments, fig.1-b. The tool and work part are eccentric by a distance E, which is the distance between the geometric center of the hole and that of the tool. The work part rotates at a speed of N. The tool moves at a federate F. It starts moving from an initial potion where it just engages the work part to a final position where it just exits the work part, as shown in fig. 1-a. The distance traveled by the tool, D, is then given by:

$$D=H_W+H_T\,, \tag{1}$$

total machining time T is given by:

$$T=\frac{D}{F\times N}. \tag{2}$$

The axial position of the tool, $x(t)$ at any time t is calculated using the following equation:

$$x(t)=F\times N_{xt}\,. \tag{3}$$

For each disc j of the tool, a facing disc of the work part i determined, where $j = 1$ to N_T, and i is between 1 and N_W, depending on the position of the tool, $x(t)$. The tool lasts at any position for at least one incremental time step Δt, depending on the feedrate F and disc height h. In the present work, Δt and h are selected so that for all feedrates, the tool would last at least $5\Delta t$ at each position.

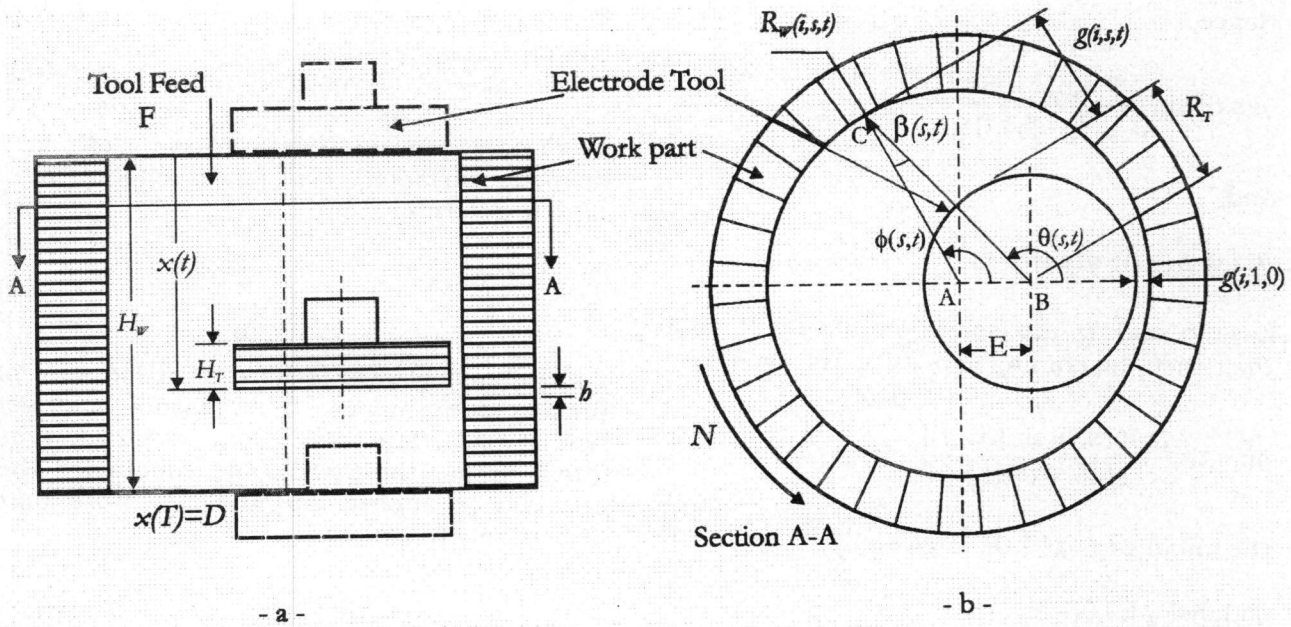

Fig. 1. Model of the orbital electrochemical hole sizing process.

At any point of time t, the distance between a segment s in disc i of the work part and the geometric center of the hole, hole radius, is expressed by the vector, $R_W(i, s, t)$. In the present work, the vector $R_W(i, s, t)$ is updated each time step and previous values of its elements are ignored. This is to save computer memory during simulation. Also, the present work is concerned with the final rather than incremental radius variations. Therefore, the suffix, t, is redundant.

After machining time t, the segment, s, will have an angular position, $\varphi(s, t)$, which is given from the following equation:

$$\varphi(s,t) = 2\pi\left(\frac{N\,t}{60} + \frac{s}{S_W}\right). \tag{4}$$

Also, after machining time t, the segment, s, will be separated by a gap $g(i, s, t)$, from the tool as shown in fig. 1-b, where $\theta(s, t)$ is the angular position of the gap around the tool. Referring to fig.1-b, and considering triangle ABC, the following relation is obtained;

$$\frac{E}{\sin(\beta(s,t))} = \frac{R_W(i,s,t)}{\sin(\pi-\theta(s,t))} = \frac{R_T + g(i,s,t)}{\sin(\varphi(s,t))}. \tag{5}$$

Hence,

$$\beta(s,t) = \sin^{-1}\frac{E\,\sin(\pi-\theta(s,t)}{R_W\,(i,s,t)} \tag{6}$$

And,

$$\theta(s,t) = \beta(s,t) + \varphi(s,t). \tag{7}$$

Eqs. (6 and 7) are solved iteratively to find $\theta(s,t)$ then, machining gap $g(i,s,t)$ is given by;

$$g(i,s,t) = \frac{R_W(i,s,t)\,\sin(\varphi(s,t))}{\sin(\pi-\theta(s,t))} - R_T. \tag{8}$$

The initial gap, $g(i,1,0)$, is given by:

$$g(i,1,0) = R_W(i,1,0) - R_T - E. \tag{9}$$

An electrolyte with conductivity k is assumed to completely fill the gap around the tool. Conductivity variations are neglected. A fully rectified AC potential of amplitude V_E and frequency f_E is applied across the electrode tool and the anode work part. Consequently, a current $I(i, s, t)$ flows in a radial direction from the work part segment s at the disc i to the tool in a plane perpendicular to hole axis. It can be given from the following equation, which is derived from model of reference [14]:

$$I(i,s,t) = \frac{R_E\,k\,h}{In(1+g(i,s,t))}. \tag{10}$$

The total current passing from the work part to the tool is obtained by summation of all work part segment currents within the work part discs facing tool discs. When the segment current passes for an incremental time period, Δt, the gap variation during that period, $\Delta g(i,s,t)$ can be given as:

$$\Delta g(i,s,t) = \sqrt{g(i,s,t)^2 + 2CV_E\Delta t} - g(i,s,t). \tag{11}$$

Where, c is a work part material constant which is given by $c = A_w k/Z_W F_a \rho_w$, where A_w is the atomic weight, Z_w is valency, ρ_W is density and F_a is Faraday's constant. Consequently, variations in the diameters of the work part can be determined at any point of time.

At the end of simulation, $t = T$, diameter variations at all work part segments are averaged to give the average work part diameter variation, ΔR_W. Linear removal rate, LRR, is determined by:

$$LRR = \frac{\Delta R_W}{T}. \tag{12}$$

Linear removal rate is used as a measure of process performance. It represents how fast hole is sized. The total volume removed, V, is given from the following equation. The equation is applied selectively to work part discs facing tool discs.

$$V = \frac{A_W}{Z_W F_a \rho_W}\sum_{t=0}^{T}\sum_{i=1}^{N_W}\sum_{s=1}^{S_W} I(i,s,t)\Delta t. \tag{13}$$

Volumetric removal rate, *VRR*, is then determined from the following eq. (14). It is taken as a measure of process performance. It is, to some extent, equivalent to *LRR*, however, it presents a conventional performance measure of machining operations. It is, also, used for calculating power consumed in machining which is a measure of process performance, that, it is not addressed in the present work.

$$VRR = \frac{V}{T}. \tag{14}$$

The simulation data, stored in the vector $R_W(i, s = 1,2,\ldots, S_w, T)$ is used to calculate roundness error *RE(i)*, or alternatively *RE*, of the hole at any disc *i*. This is accomplished by considering the following procedure:

1. Let i=1 and s=1.
2. Use elements $R_W(i,[s, s+S_w/3, 2S_w/3], T)$ to calculate a trial center of a circle that represents the hole profile, fig. 2.
3. Repeat for s = 2, 3,..., S_W.
4. Determine the range of trial centers.
5. Conduct a search within the range of trial centers to find the best center of two concentric circles which contains all hole profile points, segments radii, so that the radial distance between the two circles is minimum, *RE(i)*.
6. Roundness error is *RE(i)*.
7. Repeat for i = 2, 3,..., N_W.
8. Calculate hole average roundness error $RE_m = \frac{1}{N_W}\sum_{i=1}^{NW} RE(i)$.

Also, average straightness error of hole sides is calculated. This is done by considering segments having the same index *s* at different work part discs, $R_W(i=1,2,\ldots,N_W,s,T)$. Then, a standard straightness error calculation procedure is applied to calculate straightness error corresponding to that index, *SE(s)*, or alternatively *SE*, [15]. The straightness errors at the different indices are averaged to determine the average hole straightness error SE_m.

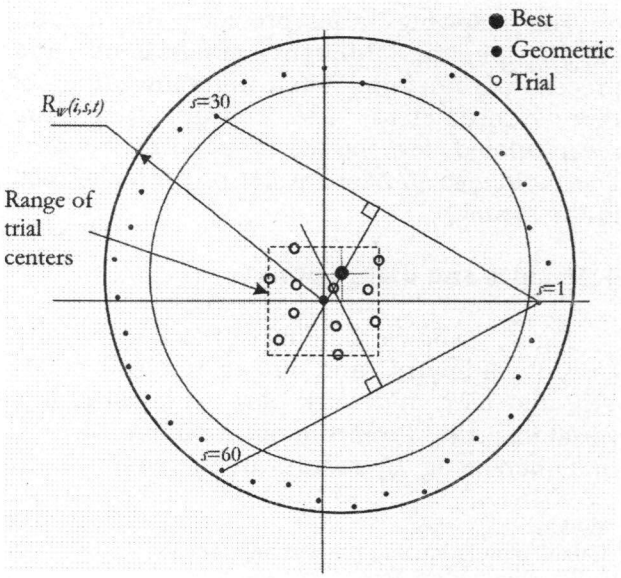

Fig. 2. Calculation of roundness error.

3. Model simulation

Model simulation is a time based one. So that, after each incremental time period, Δt, all time based model parameters are recalculated according to the following procedure:

1. Calculate tool position using eq. (3).
2. For each disc of the tool (within the work part) determine the facing work part disc.
3. Calculate angular position of the work part, eq. (4).
4. For each radial segment of each work part disc, determined from step 2, calculate the corresponding angular position on the tool using eqs. (5, 6 and 8).
5. Calculate the machining gap for each segment, eq. (7).
6. Calculate the current for each segment, eq. (10).
7. Calculate total machining current by summation of currents of all segments.
8. Calculate gap variation for each segment, eq. (11).
9. Calculate corresponding change in each work part segment radius, and update the vector *RW(i, s, t)* .
10. Stop simulation if the tool exits the work part according to eq. (1), or repeat starting with step 1.
11. If simulation stops calculate *LRR* and *VRR*. Also, calculate roundness and straightness errors and their averaged values.

The following table provides the default values for the different simulations and process parameters. When different values of these parameters are used, they are recapitulated for the corresponding results. The table also provides a list of symbols used in the model.

4. Results and discussions

Fig. 3-a shows the effect of tool lip height, H_T, on volumetric and linear removal rates, *VRR* and *LRR*, and work part averaged radius variations ΔR_W. From the figure, it can be seen that increasing H_T results in increasing both *VRR* and *LRR*. Actually, increasing H_T results in increasing the effective machining area and consequently machining current. This leads to increasing volume of material removed for the same period of time. As a result, *VRR* and *LRR* are increased. Also, from the figure, it can also be seen that increasing H_T increases ΔR_W linearly. This can be explained in shed of eqs. (10 and 13). From eq. (10), machining current is directly proportional to disc height, h, and consequently to H_T, while from eq. (13), the volume removed, V, is directly proportional to machining current.

Table 1
Default simulation and process parameters

Parameter	Symbol	Value [unit]	Parameter	Symbol	Value [unit]
Work part height	H_W	12 [mm]	Disc height	h	0.01 [mm]
Tool lip height	H_T	10 [mm]	Radial segments	S_W	90
Work part radius	R_w	8 [mm]	Work part discs	N_W	120
Radius of tool	R_T	5 [mm]	Tool discs	N_T	30
Eccentricity	E	2.25 [mm]	Time step	Δt	0.001 [sec]
Work part speed	N	95 [RPM]	Total time	T	[min]
Feedrate of tool	F	0.1 [mm/rev]	Machining time	t	[Sec.]
Atomic weight	A_w	56 [Kg/mole]	Total current	I	[Amperes]
Valency	Z_w	2 [ ]	Segment current	$I(i,s,t)$	[Amperes]
Density	ρ_w	7800 [Kg/m^3]	Position of s	$\varphi(s,t)$, $\theta(I,s,t)$	[Degrees]
Potential	V_E	21 [volts]	Tool position	$x(t)$	[mm]
Frequency	f_E	50 [Hz]	Hole radius	$R_W(i,s,t)$	[mm]
Faraday's constant	F_a	96500 [Amp.sec/mol]	Averaged radius variations	ΔR_W	[mm]
Conductivity	k	25 [1/Ω/m]	Gap	$g(I,s,t)$	[mm]
Volume removed	V	[mm^3]	Variations in gap	$\Delta g(I,s,t)$	[mm]
Linear rate	*LRR*	[μm/min]	Segment index	s	[ ]
Volumetric rate	*VRR*	[mm^3/min]	Disc index	i	[ ]
Averaged straightness error	SE_m	[μm]	Averaged roundness error	RE_m	[μm]
Straightness error	SE	[μm]	Roundness error	RE	[μm]

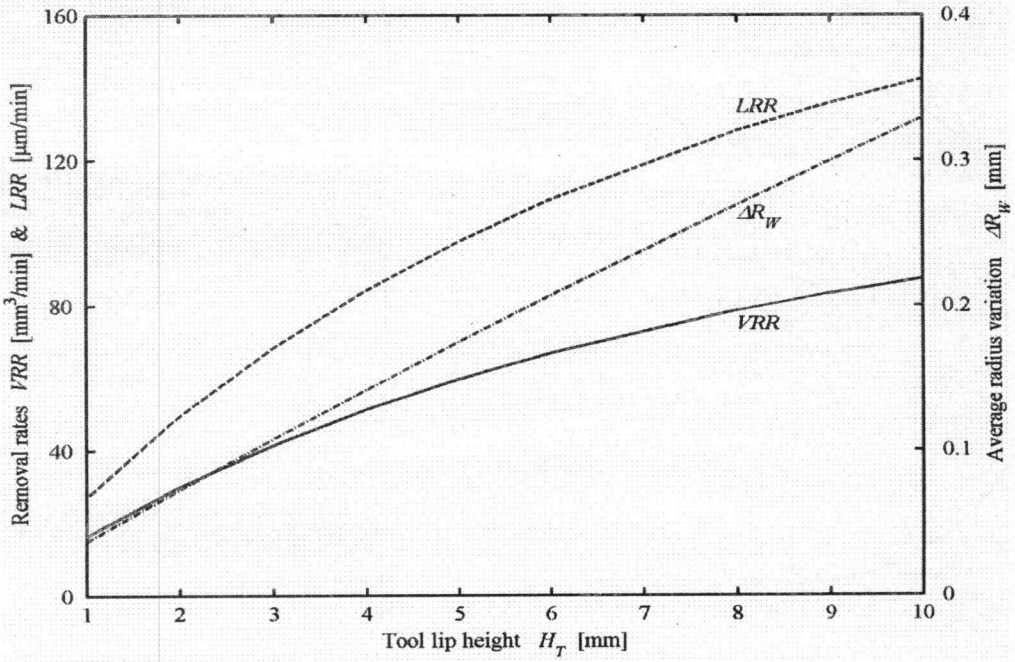

Fig. 3. Effect of tool lip height H_T on volumetric and linear removal rates *VRR* and *LRR*, and averaged work part radius variations ΔR_W.

Fig. 4-a shows two normalized radial hole profiles. A normalized radial profile is obtained by subtracting the minimum hole radius, at a certain work part disc, form the hole radii of different segments of the same disc, $R_W(i^*,s,t)-\min(R_W(i^*,s,t))$. The symbol i^* denotes a certain work part disc. In the figure, normalized profiles are obtained using discs 20 [mm] away from the top of the hole, i^*=200. The solid line profile is obtained using a tool with 1 [mm] lip height, while the dashed line profile is obtained using a tool with 10 [mm] lip height. From the figure, it can be seen that the tool with thick lip height results in larger normalized radius variations. These larger variations are due to larger amount of material removed when using the thicker lip tool. They lead to larger roundness errors, *RE*, as shown in fig. 4-b, which shows the distribution of roundness errors of work part discs along hole axis. Fig. 4-b shows that the distributions are uniform with larger values of roundness error variations for the hole machined with the thicker lip tool.

Figs. 5-a, 5-b show two normalized axial hole profiles. A normalized axial profile is obtained by subtracting the minimum hole radius, at a certain work part segment, form the hole radii of different work part discs at the same segment, $R_W(i,s^*,t)-\min(R_W(i,s^*,t))$. The symbol s^* denotes a certain work part segment. In the figure, normalized profiles are obtained using s^*= 45. The figures show that the hole machined using the thinner lip tool, H_T =1 [mm], exhibits smaller normalized radius variations, which lead to smaller straightness errors *SE*, as shown in fig. 5-c. Fig. 5-c also shows the distribution of straightness errors around the hole axis. It can be seen that the straightness error distributions are uniform. However, larger variation in the straightness error along hole axis are obtained when the thinner lip tool is used.

Fig. 6 shows the effect of H_T on averaged roundness and straightness errors. From the figure, it can be seen that increasing H_T increases both RE_m and SE_m. However, the increase in RE_m is more uniform. The nonuniform increase in SE_m can be attributed to the interactions of the numerical values of machining parameters, *N* and *F*, and those of simulation parameters *h* and S_W. Further statistical analysis of these interactions is necessary; however, it is not pursued in the present work.

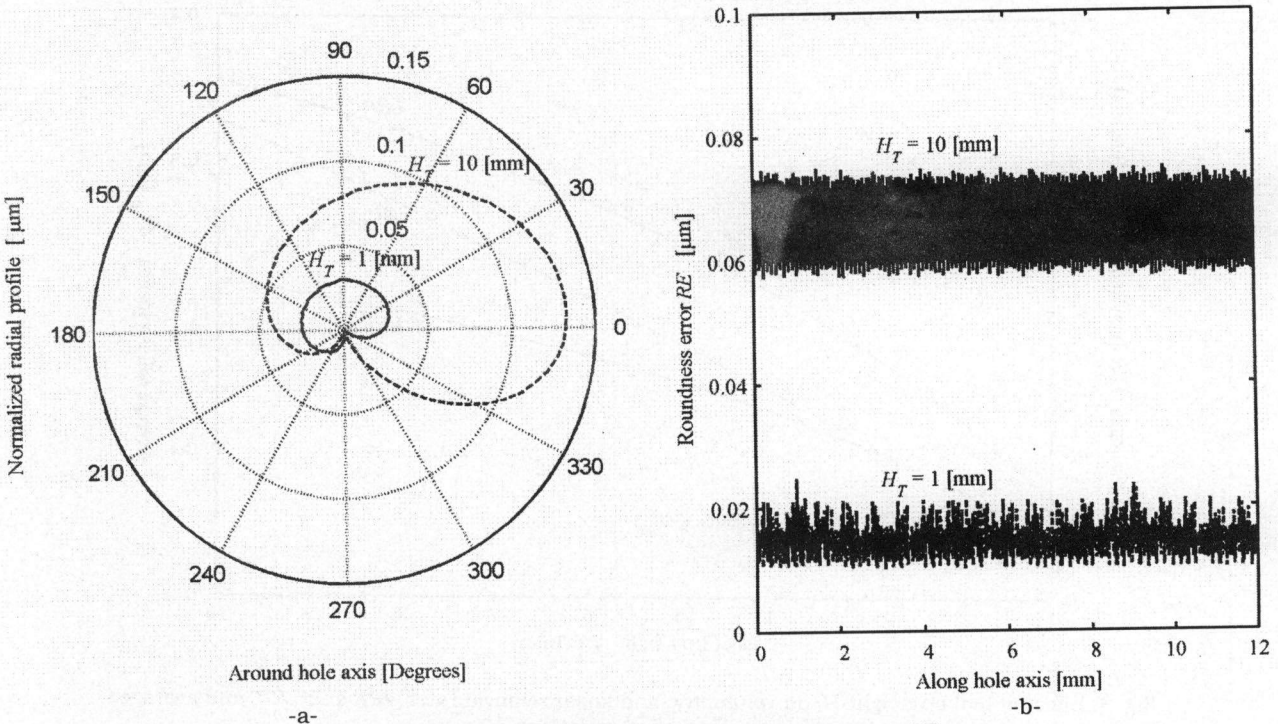

Fig. 4. Effect of tool lip height H_T on roundness errors *RE*.

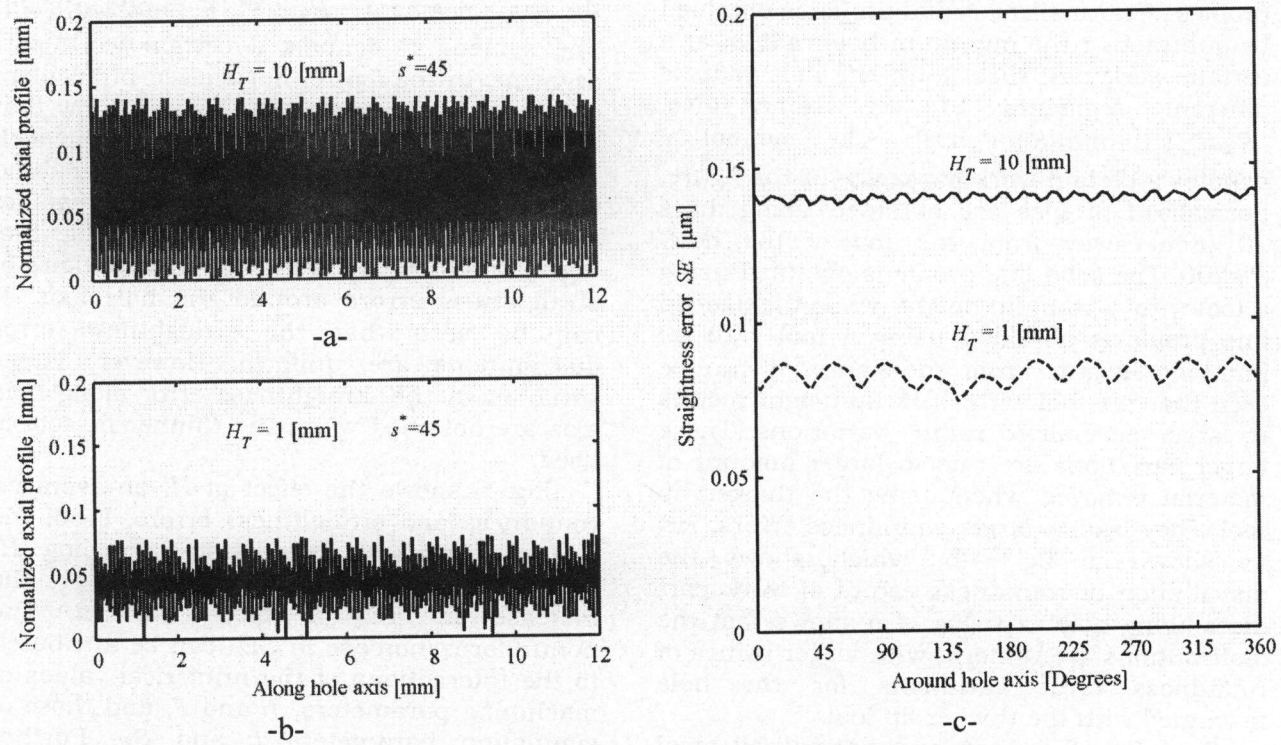

Fig. 5. Effect of tool lip height H_T on distribution of hole roundness error *RE*.

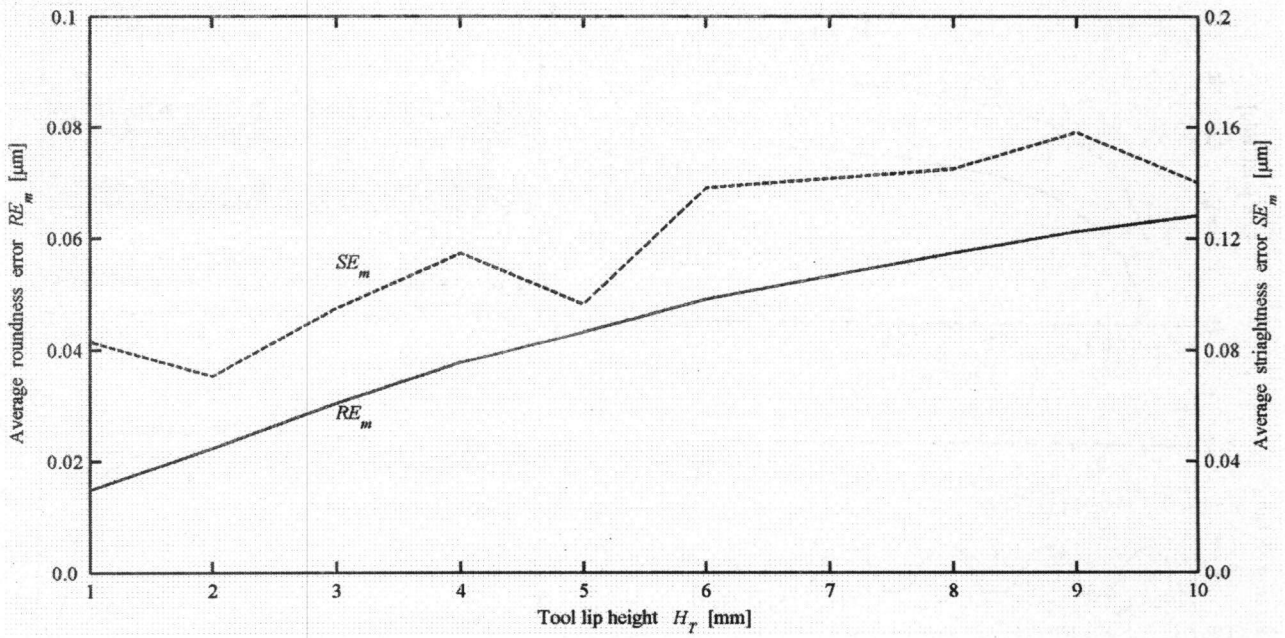

Fig. 6. Effect of tool lip height H_T on averaged roundness RE_m and straightness SE_m errors.

The effect of federate F on volumetric and linear removal rates *VRR* and *LRR* is shown in Figs. 7-a. From the figure, it can be seen that increasing F by ten folds, from 0.05 to 0.5, increases *VRR* and *LRR* by only 7.5. Obviously, the effect of F on *VRR* and *LRR* is marginal. This result is expected as increasing F decreases both machined volume and machining time which make up *VRR* and *LRR*. Figs. 7-b shows the distribution of roundness error along hole axis for different feedrates. From the figure, it can be seen that increasing feedrate decreases roundness error, due to the subtle amount of material machined and the consequent small variations in hole radius. Similar trend can be observed for the straightness error distribution around the hole axis, Fig.7-c. Fig. 7-d shows the effect of federate F on average roundness and straightness errors, RE_m and SE_m. From the figure, it can be seen that increasing feedrate decreases average errors up to about F= 0.3. Increasing feedrate beyond this limit results in a considerable increase in the average errors. In this case the tool cuts a helical groove in the surface of the hole rather than machining a cylindrical surface, which leads to the increased average errors. Further increase in the feedrate results in almost no material removed and consequently average errors drops as the simulation assumes a true hole at t = 0.

Fig. 8 shows the variations in machining current, I, over time using different process parameters. Figs. 8-a shows the simulated actual and averaged (filtered) I, for a tool having H_T =8. The averaging process is obtained using a 9th low pass filter with 10 Hz cut off frequency. It is more representative to use average current rather than rectified AC current in comparing current levels in simulation results. Fig. 8-b shows the simulated machining currents for three tools with H_T = 1, 3, 8 respectively. The figure shows that thick tools results in higher average machining currents. By considering the levels of the average current and tool lip height, it can be seen that the average current level is proportional to tool lip height. This is in compliance with eq. (10) where disc current $I(i,s,t)$ is directly proportion to disc height h. Figs. 8-c and 8-d show that F and N have no effect on the level of average current. However, fig. 8-d shows that increasing R_T results in an increased current level. This is because increasing R_T results in decreasing the machining gap around the tool which results in increasing machining current.

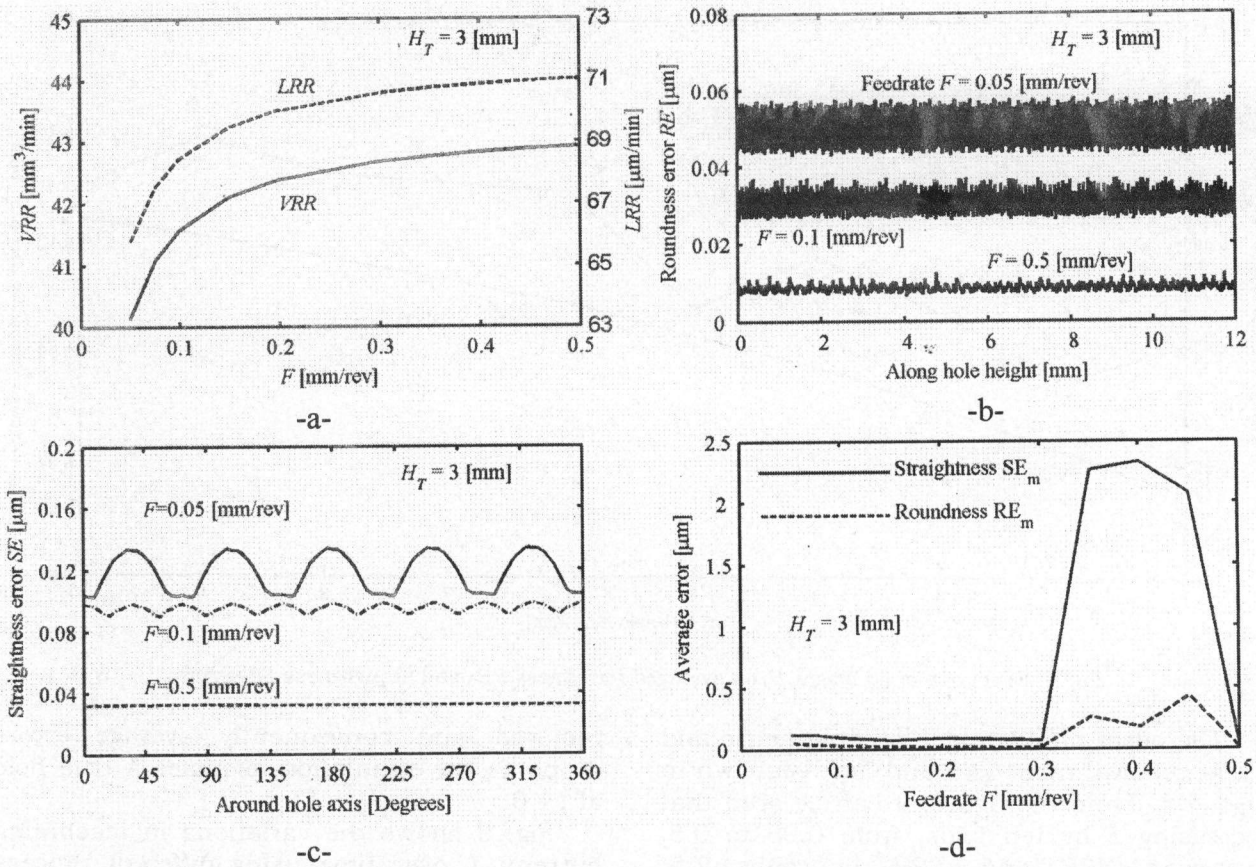

Fig. 7. Effect of Feedrate F on volumetric and linear removal rates *VRR* and *LRR*, and averaged roundness and straightness errors RE_m and SE_m.

Fig. 9 shows the effect of N on *VRR* and *LRR*, and average errors. From fig. 9-a, it is clear that the effect of N on *VRR* and *LRR* is negligible. Increasing N, from 10 to 500, resulted in almost no increase in *VRR* and *LRR*; Perhaps a subtle increase at low N. At small N, say 0, the tool machines a narrow region from the surface of the hole and consequently material removed is small. Increasing N allows the tool to machine from all sides of the hole resulting in an increase in material removed and consequently *VRR* and *LRR*. Further increase in N would not have any effect as the tool still remove material from all sides of the hole; however, more averaging of machining would take place. The feedrates in the figure is expressed as [mm/min] rather than [mm/rev] as there are variations in N.

The effect of N on the distribution of *RE* and *SE* along and around hole axis are shown in figs. 9-b and 9-c. From the figures, it can be seen that at small N, *RE* and *SE* are relatively large with more variations in their values. On the other hand, at large N, *RE* and *SE* are relatively small with almost no variations in their values. Again, this is due to the averaging effect of the orbiting speed on machining process. The effect of N on average straightness and roundness errors is shown in fig. 9-d. Increasing N, results in a sharp decrease in average roundness and straightness errors especially at small N. This is due to the increase in the averaging effect of the orbital motion of the work part on the machining rate at the sides of the hole.

Fig. 10-a shows the effect of tool radius R_T on *VRR* and *LRR*. From the figure, it can be seen that increasing R_T results in decreasing *VRR* and *LRR* up to R_T = 3. Increasing R_T, beyond 4 mm, results in an increase of *VRR* and *LRR*. An explanation of this result can be given in terms of current density distribution which is shown in fig. 10-b. The current density distribution is determined at an

arbitrary disc of the work part at an arbitrary time during machining. It is given for R_T = 0.5, 4, 7. It is clear from the figure that the current density for R_T = 4 is lower than those for R_T = 0.5 and for R_T = 7. This implies that a range of tool radius should be avoided to increase process productivity as expressed by *VRR* and *LRR*.

Figs. 11-a and 11-b show the *SE* and *RE* distributions along and around the hole axis, respectively, for different values of tool radius R_T. Fig. 11-a shows that for R_T = 4, straightness error is small with larger variation in its value. At this radius, minimum material was removed due to the low current density as explained earlier. However, fig. 11-b shows that, at the same R_T, the roundness error is maximum. This is due to the large variation in current density, fig. 10-b which leads to non uniform machining around hole axis. Fig. 11-c shows the variations in average RE_m and SE_m errors with tool radius R_T. The figure shows that there is a local minimum of SE_m average error while there is a local maximum of RE_m average error at R_T = 4. This means that the effects of tool radius R_T on RE_m and SE_m errors are contradicting.

The effect of eccentricity *E* on *VRR* and *LRR* is shown in fig. 12-a. From the figure, it can be seen generally that increasing *E* increases *VRR* and *LRR*. However, for smaller *E*, the increase is minor, while, for larger *E*, the increase in larger. This is because increasing *E* results in a corresponding decrease in the machining gap and more localized machining. The effect of *E* on average straightness and roundness errors are shown in fig. 12-b, which indicates that roundness error is more susceptible to *E* compared with straightness error. This can be reduced to fact that *E* varies in radial direction and consequently it has more effect on roundness error.

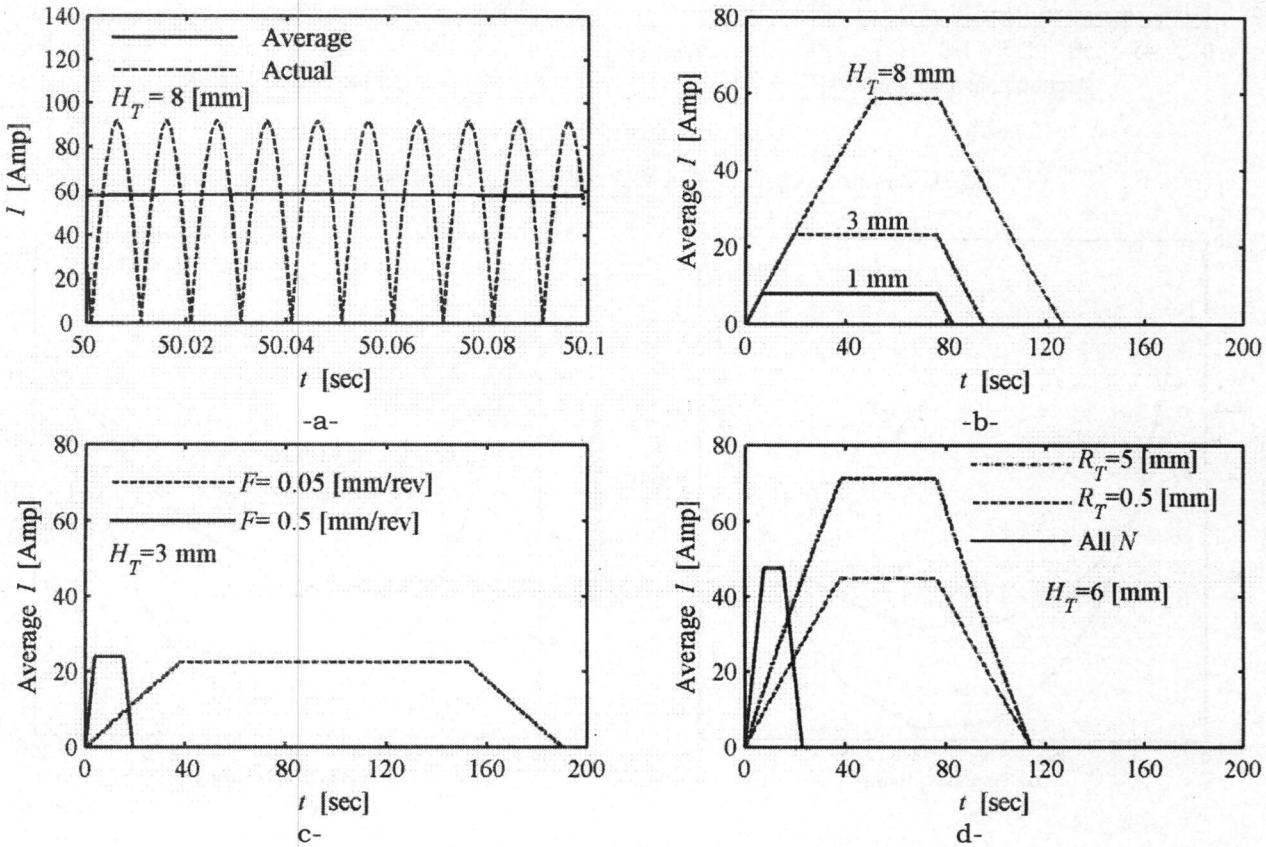

Fig. 8. Effect of process parameters on machining current.

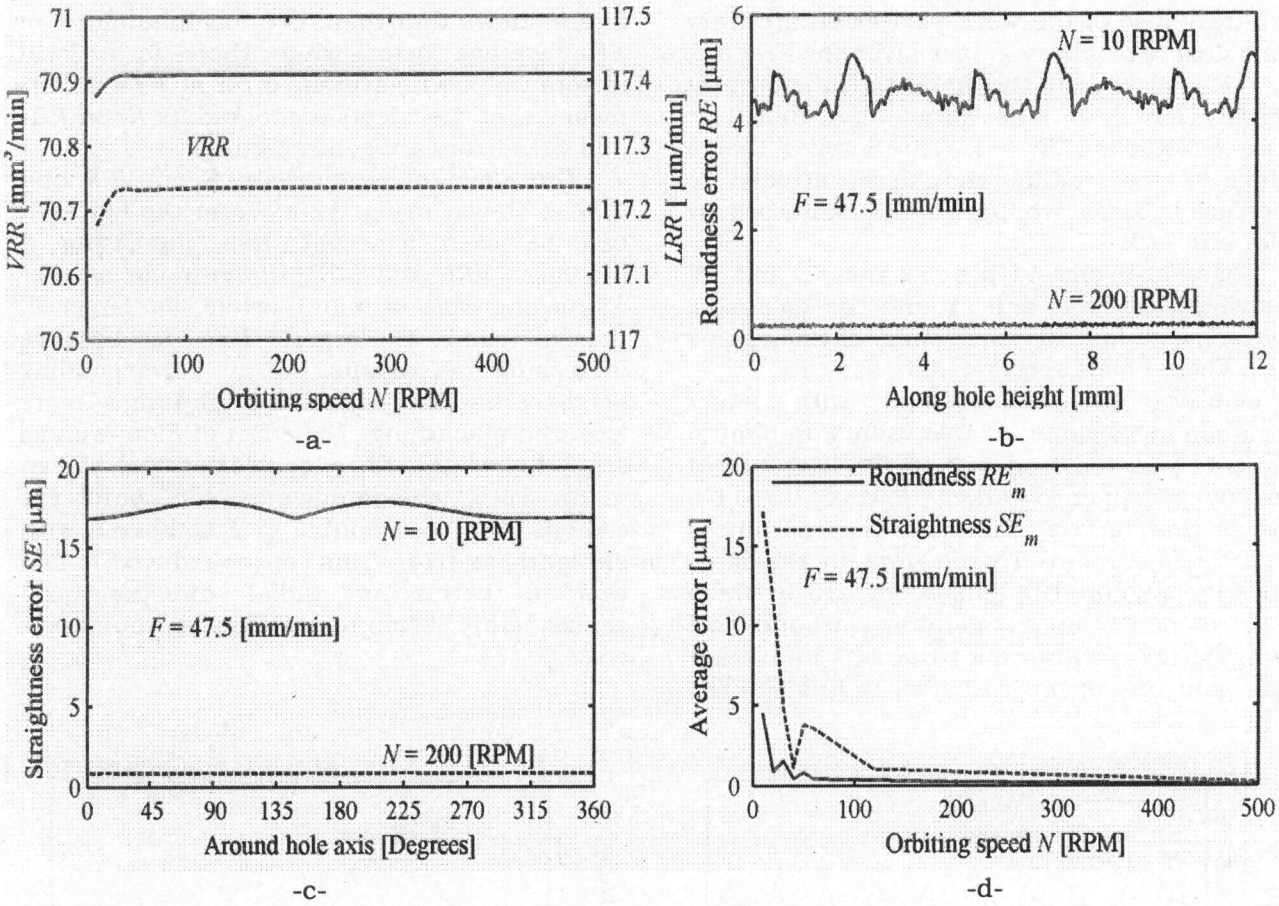

Fig. 9. Simulated effect of N on *VRR* and *LRR* and average errors.

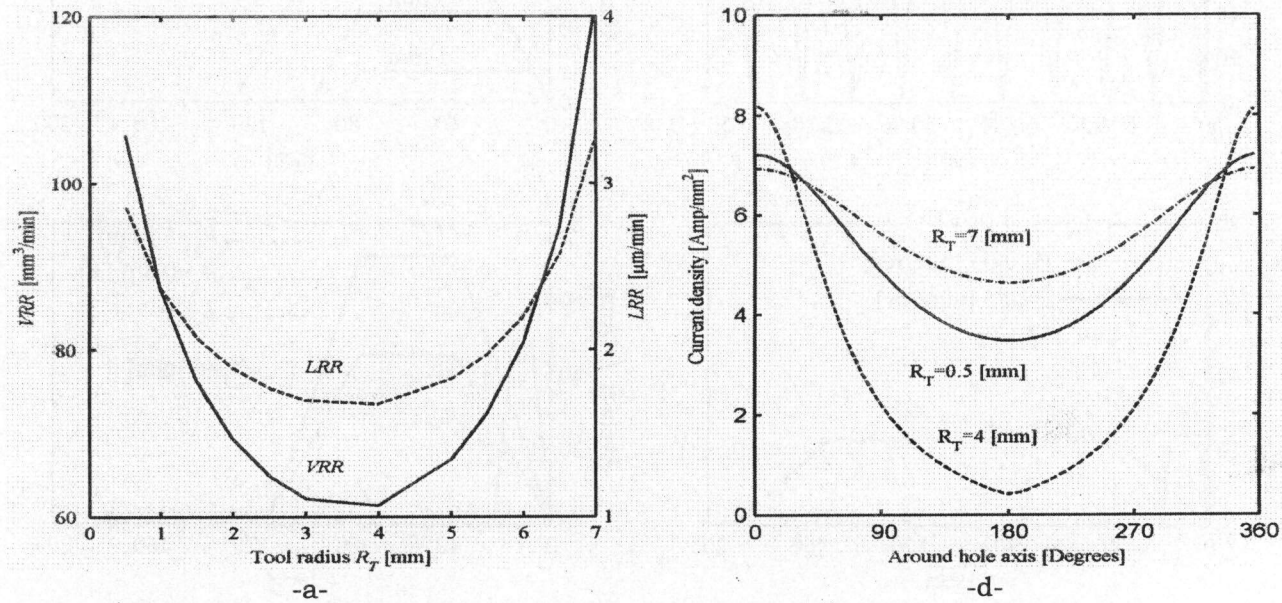

Fig. 10. Effect of R_T on *VRR*, *LRR* and average errors.

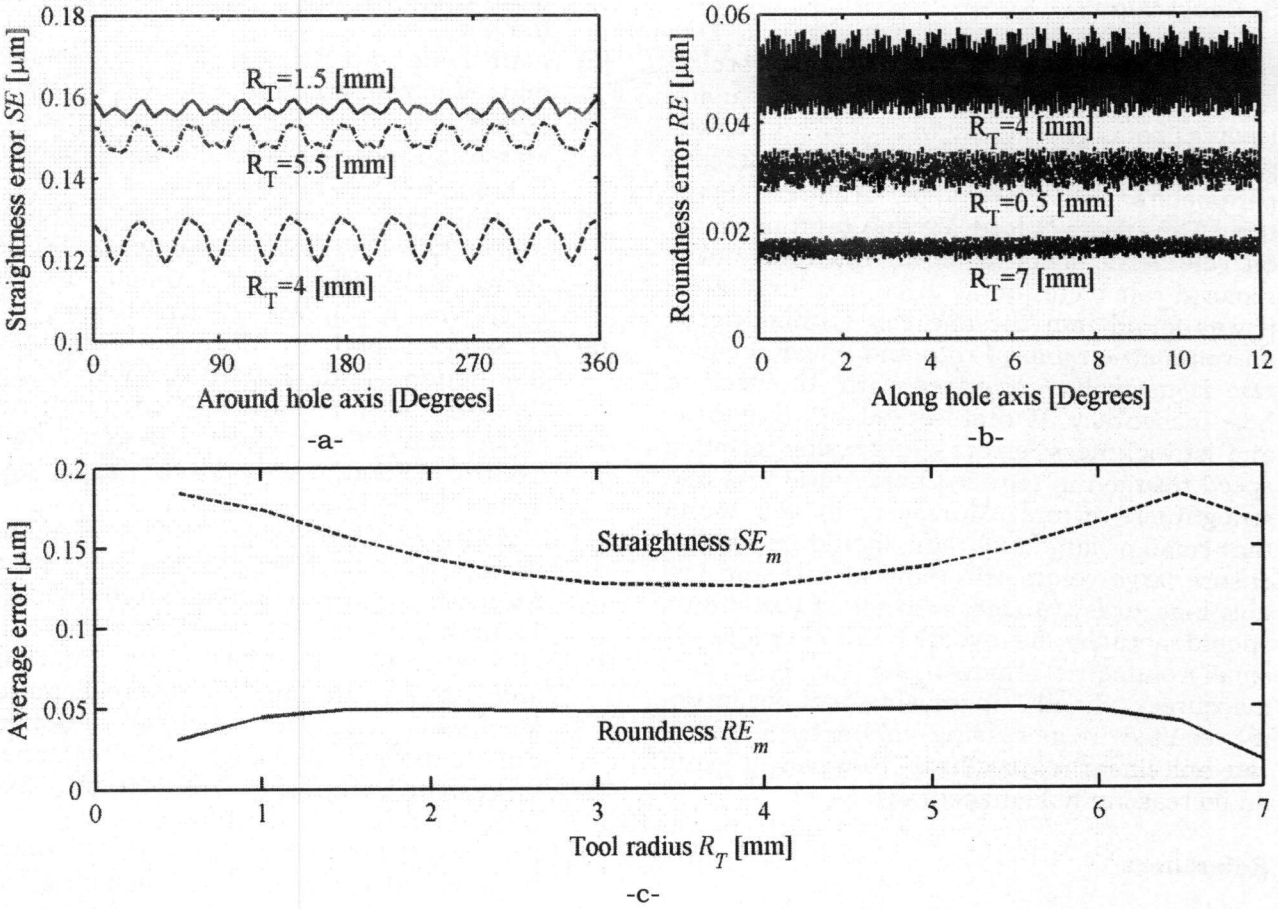

Fig. 11. Effect of tool radius R_T on average errors.

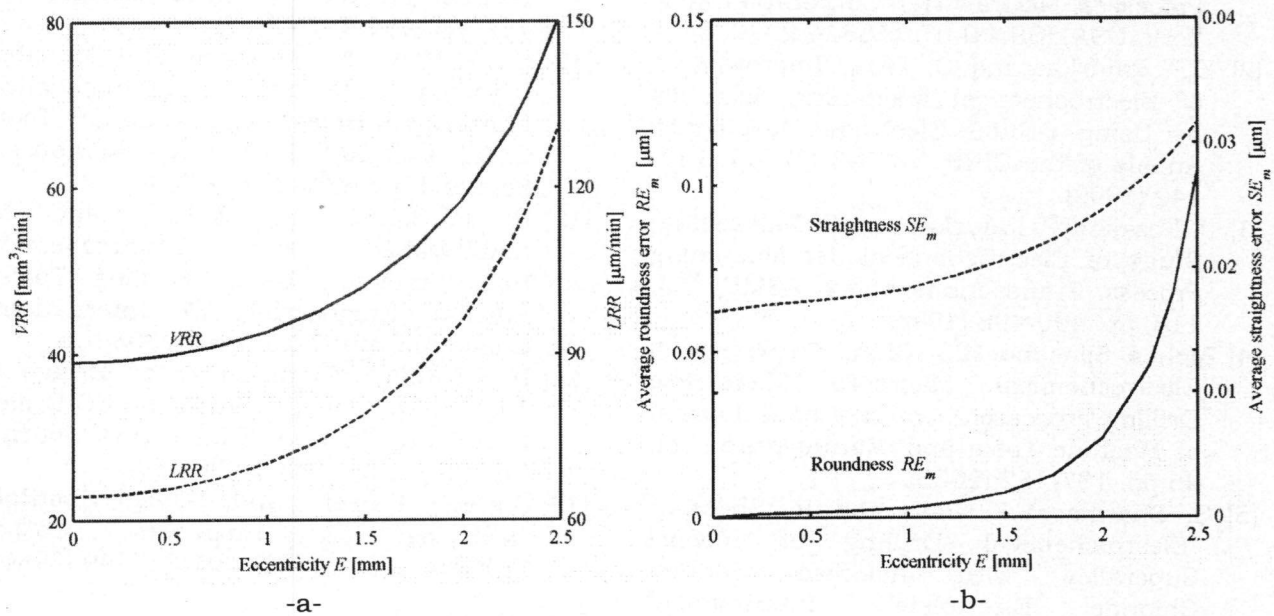

Fig. 12. Effect of eccentricity E on *VRR, LRR* and average errors.

5. Conclusions

This work presented a model for the orbital electrochemical hole sizing process; using feeding tools. The model was used to investigate the correlation between different process parameters and process performance measures. The effects of feedrate and orbiting speed on volumetric metal removal rate and linear removal rate were found to be marginal. Also, it was found that the effect of orbiting speed on volumetric removal rate and linear removal rate is negligible compared with its effect on hole inaccuracy as represented by roundness and straightness errors. Increasing orbiting speed resulted in reduced hole roundness and straightness errors. Moreover, it was found that small or large tool radii should be used to ensure large volumetric removal rate and low hole inaccuracy. A certain range of tool radius should actually be avoided as it results in small volumetric removal rate and large hole inaccuracy. Finally, increasing tool eccentricity resulted in increasing volumetric removal rate and linear removal rate. However, it led to an increase in hole inaccuracy.

References

[1] H. El-Hofy, Advanced Machining Processes, Non-Traditional and Hybrid Processes, McGraw Hill. Corporation, New York, USA, ISBN 0-07-145334-2 (2005).

[2] K.P. Rajurkar and D. Zhu, "Improvement of Electrochemical Machining Accuracy by Using Orbital Electrode Movement", Annals of the CIRP, Vol. 48 (1), pp. 139-142 (1999).

[3] J. Kozak, K.P. Rajurkar and R. Balkrishna, Study of Electrochemical Jet Machining Process. Transactions of the ASME, Vol. 118, pp. 490-498 (1996).

[4] Mohen Sen and H.S. Shan, "A Review of Electrochemical Macro-To Micro-Hole Drilling Processes", International Journal of Machine Tools and Manufacture, Vol. 45 pp. 137-152 (2005).

[5] S. Sharma, V.K. Jain and R. Shekhar, "Electrochemical Drilling of Inconel Superalloy with Acidified Sodium Chloride Electrolyte", International Journal of Machine Tools and Manufacture, Vol. 19, pp. 492-500 (2002).

[6] H. Hocheng and P.S. Pa, "Electropolishing and Electrobrightening of Holes Using Different Feeding Electrodes", Journal of Material Processing Technology, Vol. 89 (90) pp. 440-446 (1999).

[7] T. Masuzawa and S. Sakai, "Quick Finishing of WEDM Products by ECM Using Mate Electrodes", Annals of the CIRP, Vol. 36 (1), pp. 123-126 (1999).

[8] E. Soliman and H. El-Hofy, "Computer Simulation of the Electrochemical Sizing Process", 7th International Conference on Production Engineering Design and Control PEDAC, Alexandria, Egypt, pp. 1111-1121 (2001).

[9] J. Kozak, L. Dabrowiski and H. Osman, "Computer Modelling with Rotating Electrode", Journal of Material Processing Technology, Vol. 28, pp. 157-167 (1991).

[10] M.S. Hewidy, S.J. Ebied, K.P. Rajurkar and M.F. El-Safti, "Electrochemical Machining Under Orbital Motion Conditions", Journal of Material Processing Technology, Vol. 109, pp. 339-346 (2001).

[11] Z. Sadollah Bamerni and H. El-Hofy, "Orbital Electrochemical Machining of Electrodischarge Machined Surfaces", Advanced Manufacturing Systems and Technology. CIST Courses Lectures No. 437, pp. 464-487 (2002).

[12] H. El-Hofy, N. Al-Salem and M. Abd-ElWahed, "Orbital Electrochemical Finishing of Holes Using Stationary Tool", CAPE- Vol. 10, 18-19 March, Edinburgh, Scotland, pp. 169-177 (2003).

[13] N. Al-Salem, H. El-Hofy and M. AbdElWahed, "Orbital Electrochemical Hole Finishing Using Feeding Tools", AlAzhar Engineering 7th International Conference pp. 7-10 April (2003).

[14] H. El-Hofy, "Computer Aided Design of Tool Shape for EC-Sizing of EC-Drilled Holes", Alexandria Engineering Journal Vol. 28 (3), pp. 383-402 (1989).

[15] J.F.W. Galyer and C.R. ShotBolt, "Metrology for Engineers", Cassell Publishers Ltd, ISBN 0304317349 (1990).

Received May 30, 2007
Accepted September 2, 2007